Researches in Interplanetary Transfer

JOHN V. BREAKWELL,[1]
ROLLIN W. GILLESPIE[2]
and STANLEY ROSS[3]

Lockheed Missiles and Space Div.
Sunnyvale, Calif.

A method is presented by which interplanetary trajectories may be calculated extremely rapidly and to a degree of accuracy suitable for design studies. By splitting the three-center problem associated with interorbital ballistic transfer into three one-center segments which overlap somewhat at their junctions, solutions may readily be found by machine iteration. The extreme speed of the method enables wholesale amounts of worthwhile numerical results to be obtained. Examples presented in the paper include velocity requirements for trips to and from Mars during the year 1960. Considering that the orbits of Earth and Mars are elliptical and mutually inclined, the Hohmann minimum energy transfer criterion disappears, and the occurrence of several local minimum energy trajectories is observed; this phenomenon is expected to be typical of all interplanetary orbit studies.

WITH the advent of interplanetary voyages, it becomes important to have at hand complete information regarding velocity requirements for journeys between the various planets. If comprehensive data of this nature are made available, they can provide a useful basis for analyzing propulsion requirements, for planning ultimate system configurations, and for conducting feasibility studies relating to any mission contemplated. What is required is a method of calculation rapid enough to allow wholesale amounts of computations to be performed cheaply and efficiently, yet whose accuracy need be limited only to a degree expected in design studies.

It is natural, when such moderate accuracy is required, to approximate the single three-center ballistic problem by three distinct one-center motions, the latter being soluble in closed form (4).[4] Instead of joining conic segments at particular radial distances, the solution is constructed by imagining the heliocentric segment extending to the very centers of the terminal planets, whereas each planet-centered hyperbola meeting the heliocentric arc does so at its asymptote. This construction materially simplifies the calculation procedure and is expected to introduce only tolerable amounts of error into the computations.

By employing a high speed computer to fabricate the combined solutions, literally thousands of orbits per hour may be calculated, and their parameters presented in standardized charts and tables for the various solar planets. These may then be consulted to find the launch, midcourse and arrival information relating to a variety of missions.

A gridwork is selected, each of whose points corresponds to a particular departure date and a specific transfer time. Upon these points are overlaid contours of constant departure speed, constant arrival speed or other quantities of interest. These plots may be readily scanned, not only to select optimum trips for any given mission, but also to observe tradeoff relations for nonoptimal trips.

It is supposed that the planets are moving in fixed ellipses around the sun, every two orbits mutually inclined at some particular angle. Upon selection of appropriate ellipse parameters for the time interval of interest (7–9), preliminary input data may be readily computed by the machine. Following the approach of (2), a modified form of Lambert's theorem is then utilized to find the energies of all heliocentric arcs connecting the departure and arrival planets at the correct dates. For transfer arcs with included central angle $\leq 2\pi$, it is shown that exactly two such segments exist for any specified pair of dates, one orbit aimed with and the other against the departure planet's orbital motion; each time the central angle increases by 2π, up to four further solutions are added.

After the proper energies are determined, the heliocentric velocities at both ends of the arc are evaluated. These values are transformed into relative vector velocities at the planets by subtracting the motions of the latter bodies. The right ascensions, declinations and speeds corresponding to such "hyperbolic excess velocities" are listed as outputs, together with the useful heliocentric data for the flight.

Total average computing time for each orbit amounts to approximately 0.1 sec on the IBM 7090, using Fortran. All variables are expressed in nondimensional form; lengths are normalized with respect to the astronomical unit, speeds with respect to Earth's mean orbital speed.

Analysis of Results

It is instructive to begin by considering the transfer problem under the assumption that the planetary orbits be coplanar, concentric circles. Fig. 1 illustrates contours of constant hyperbolic excess departure speeds for trips to Mars. Departure dates cover the period from March 1960 to April 1961, a span which straddles the planetary opposition of Jan. 1, 1961.

All transfer arcs are co-planar with the planetary motions, with the exception of those described by the dashed lines. These latter trips involve central transfer angles of 180 deg, and the planes of transfer for journeys of this type may be inclined at any arbitrary angle to the two planets' motions. Since to any point on the dashed lines there corresponds a multiplicity of transfer orbit inclinations, it follows that each point represents a variety of departure velocities. The dashed lines are therefore singular in nature and will be seen to have additional significance in the more realistic cases to be discussed following. Viewing Fig. 1 as a geodetic contour map, these dashed lines correspond to sharp ridges of negligible thickness, having maximum heights determined by the largest values of departure velocity, i.e., by trips leaving perpendicularly to the ecliptic plane (rearward, or retrograde launchings are not shown in Fig. 1).

Presented at the ARS 14th Annual Meeting, Washington, D.C., Nov. 16–20, 1959.

[1] Staff Scientist.
[2] Research Specialist. Member ARS.
[3] Research Scientist. Member ARS.
[4] Numbers in parentheses indicate References at end of paper.

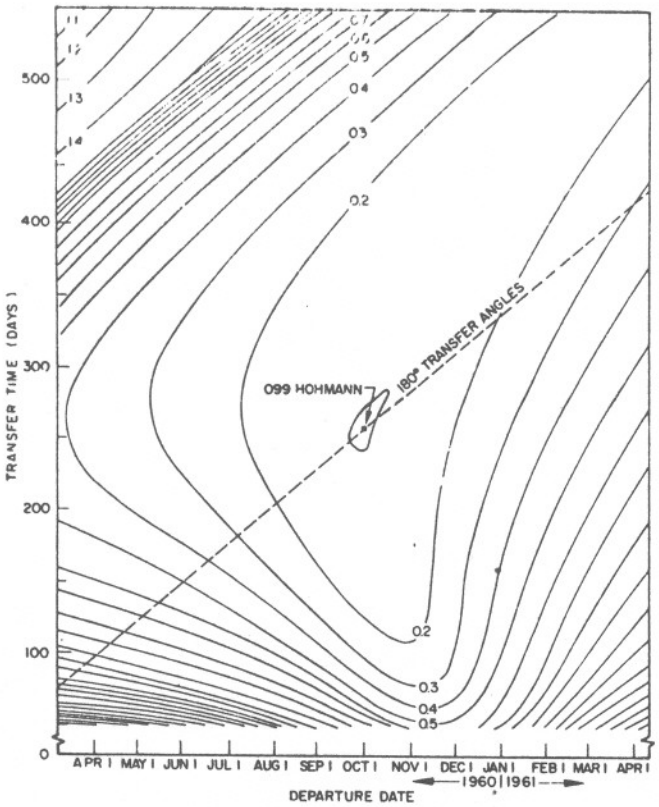

Fig. 1 Earth to Mars (co-planar, circular planetary orbits). Hyperbolic excess departure speeds (increments of 0.1). Normalized with respect to Earth's mean orbital speed

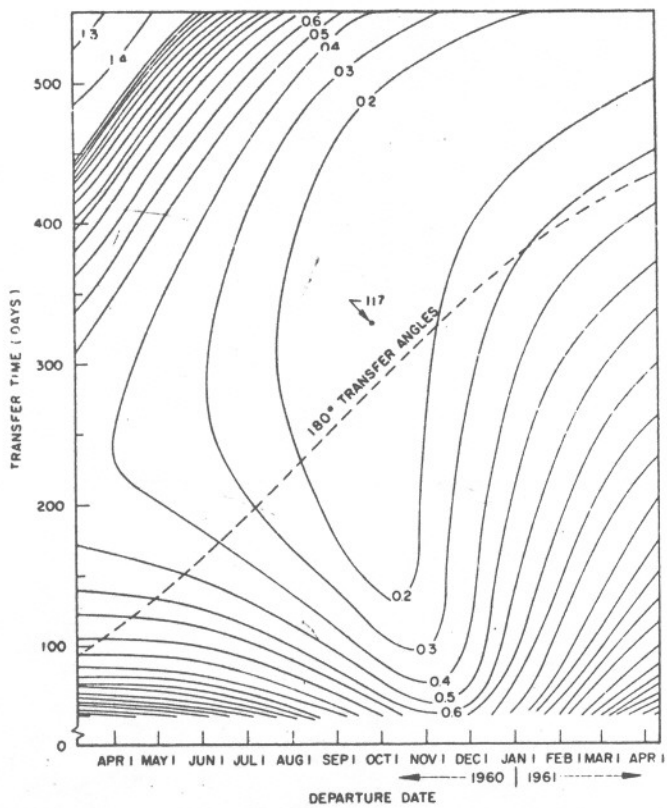

Fig. 2 Earth to Mars (co-planar, elliptical planetary orbits). Hyperbolic excess departure speeds (increments of 0.1). Normalized with respect to Earth's mean orbital speed

The equations of such lines in general are determined by the relation between departure and arrival times for 180-deg transfer. Using L_1 and L_2 to denote planetary longitudes measured from an arbitrary fixed line in space, we have

$$L_2 = \pi + L_1$$

and therefore that

$$d(\Delta t)/dt_1 = n_1/n_2 - 1$$

where

t_1 = departure date
Δt = transfer time
n_1, n_2 = respective planetary mean motions

For trips from Earth to Mars, the slope is about 0.88, for return orbits −0.468.

In close agreement with (3 and 4), the "Hohmann" point of minimum departure speed is found at Oct. 1, 1960, with an associated journey of 259 days. Since this is a trip involving a transfer angle of 180 deg, it also lies on the dashed line ridge.

Thus, it is found that the ridges corresponding to 180-deg transfer occur once every synodic period, each passing through a Hohmann point, and each having a slope of $n_1/n_2 - 1$. An infinite number of these equally spaced lines exist and may be found by expanding the figure's scope. The greater the difference in mean motions between the two planets, the shorter the synodic period, and therefore the closer the spacing of these dashed lines.

Another type of ridge may be observed in Fig. 1, occurring in the upper left-hand corner. This corresponds to transfer angles of 0 or 360 deg. Its direction is also given by $n_1/n_2 - 1$ although the contours here build up somewhat more gently than those for 180-deg transfer. The two types of ridges displayed in Fig. 1 are to be found evenly interspersed between one another.

As a matter of fact, *any* particular line drawn with a slope of $n_1/n_2 - 1$ represents an infinitude of transfers between the two planets, each of which involves the same transfer angle. However, successive points on any such line correspond to transfers of longer and longer duration. Following any one line upward, we find that its associated solutions steadily approach parabolic arcs, all of which traverse the same transfer angle. We conclude, therefore, that for long transfer times[5] the contours of constant departure speed asymptotically approach straight lines parallel to the ridges.

Fig. 2 describes the situation when planetary orbit eccentricities are introduced. Both orbits are still assumed to be co-planar. The date for minimum departure speed has shifted to Sept. 26, 1960, and it no longer involves a transfer of 180 deg (the transfer angle is now about 210 deg). Travel time for this point has increased to 360 days, whereas the speed itself has changed from a value of 0.099 n Fig. 1 to the presently indicated value of 0.117. This increase of 18 per cent illustrates the disadvantages in basing calculations on the "Hohmann" type of analysis. Note also that the ridges, as well as the constant velocity asymptotes, have become undulating lines, owing to the introduction of orbital eccentricities.

Fig. 3 is similar in nature to Fig. 15 of (3), with refinements having been introduced here by the choice of a finer grid size. It illustrates the consequences of introducing planetary orbit inclinations as well as eccentricities into the problem.

The chief resulting modification is observable near the lowest ridge, which has now broadened. The summit line no longer represents orbits perpendicular to the departure plane, but arises from a rather more complicated relation for those points at which a balance is achieved between forward and retrograde firings.

Since the mutual inclination between the orbits of Earth

[5] Figs. 1 to 8 do not include results for transfer through more than 360 deg.

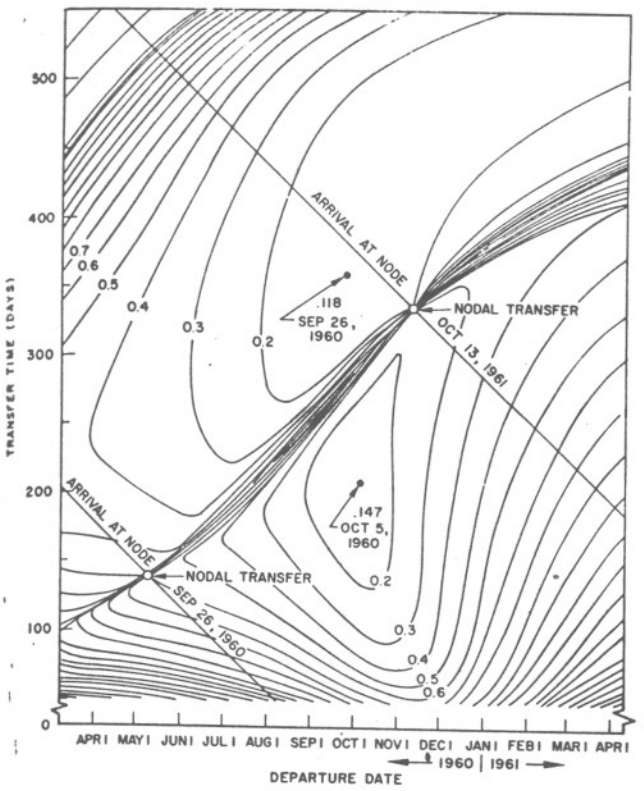

Fig. 3 Earth to Mars. Hyperbolic excess departure speeds (increments of 0.1). Normalized with respect to Earth's mean orbital speed

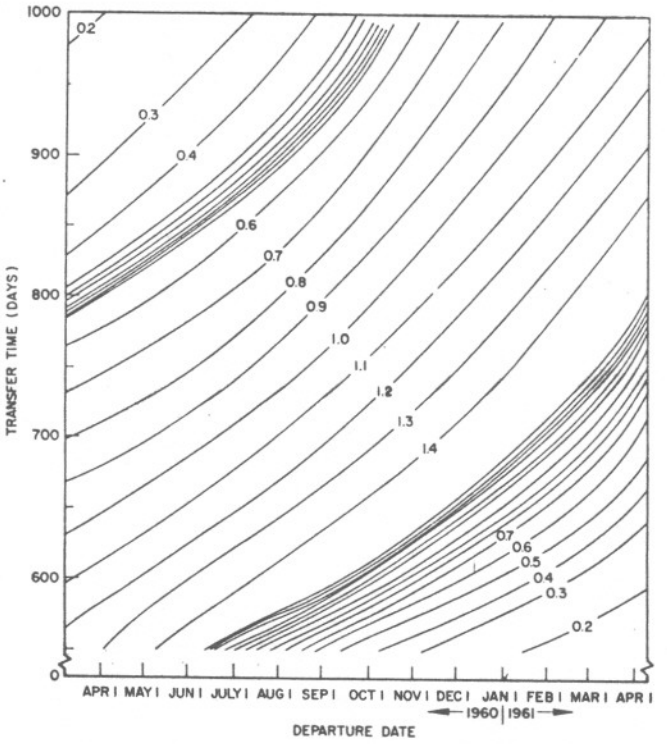

Fig. 4 Earth to Mars, long transfer times. Hyperbolic excess departure speeds (increments of 0.1). Normalized with respect to Earth's mean orbital speed

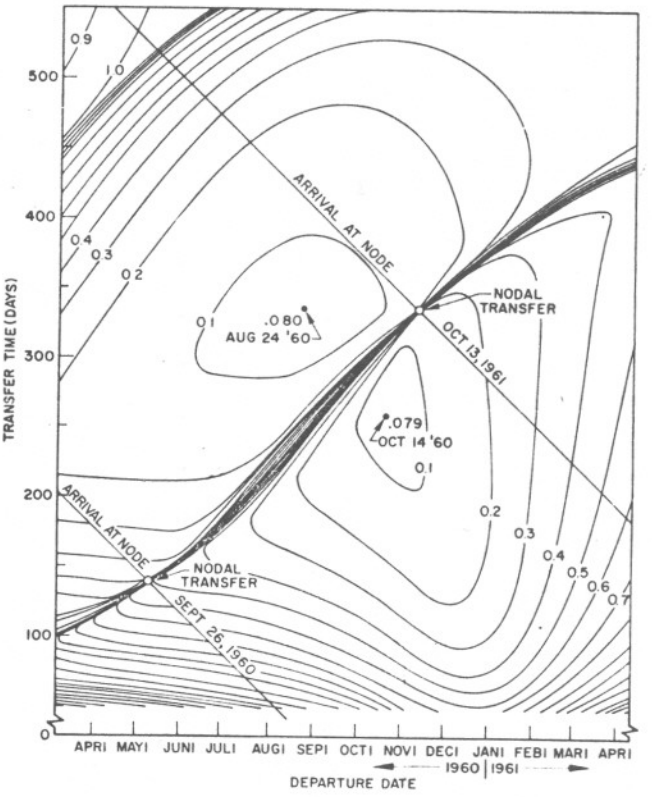

Fig. 5 Earth to Mars. Hyperbolic excess arrival speeds (increments of 0.1). Normalized with respect to Earth's mean orbital speed

and Mars is quite small (about 2 deg), this particular ridge is still narrow, and since the eccentricities of both planetary orbits are small, its undulations are also limited. Vestiges of the co-planar transfer model remain at the points of nodal transfer for which many similar orbits are possible, each with a different inclination to the ecliptic.

It is convenient to imagine Fig. 3 to have arisen from Fig. 2 by having held the nodal transfer points clamped and having a wedge forced up from below the thin ridge. This useful analogy is further validated by the fact that the disturbance is indeed localized in the vicinity of the ridge. At points moderately far removed from this ridge, the contours for Figs. 2 and 3 agree closely.

Now the original Hohmann point of Fig. 1 has bifurcated into two local minimum orbits, these occurring at about ± 5 days from Oct. 1, 1960. The smaller of the two in value, 0.118, is only 1 per cent different from its value in Fig. 2. The other, 0.147 (a trip of 209-days duration) arose purely as a result of introducing relative orbital inclinations. The former point, incidentally, corresponds to an orbit which lies almost in the ecliptic plane, having a transfer angle of about 220 deg. This particular trip leaves Earth at approximately the time when Mars is at the ascending node, and arrives at Mars when it is at the descending node.

These nodal arrival lines, together with the ridges, subdivide the diagram into diamond-shaped regions. In adjacent segments, the character of the motion alternates between orbits aimed above and those aimed below the ecliptic plane.

Although the overall character of the curves is similar for each synodic period, particular details vary from one opposition to the next. Thus, for the period 1966–1968, for instance, the overall minimum departure velocity is 0.098, considerably lower than the present one, and evidently smaller in value than the Hohmann case! The apparent discrepancy is a result of the planetary orbit eccentricities and the fact that Mars' mean (and not its minimum) radius was chosen for the Hohmann analysis of Fig. 1.

A final point of interest concerning this phase of the trips is shown in Fig. 4, which depicts the asymptotic solutions for long transfer time. These curves, as explained previously, are all virtually parallel to the ridges. Such regions are of possible interest for nonstop round-trip journeys on which an unfavorable return region from Mars may be encountered for the shorter trips going, but not for the longer.

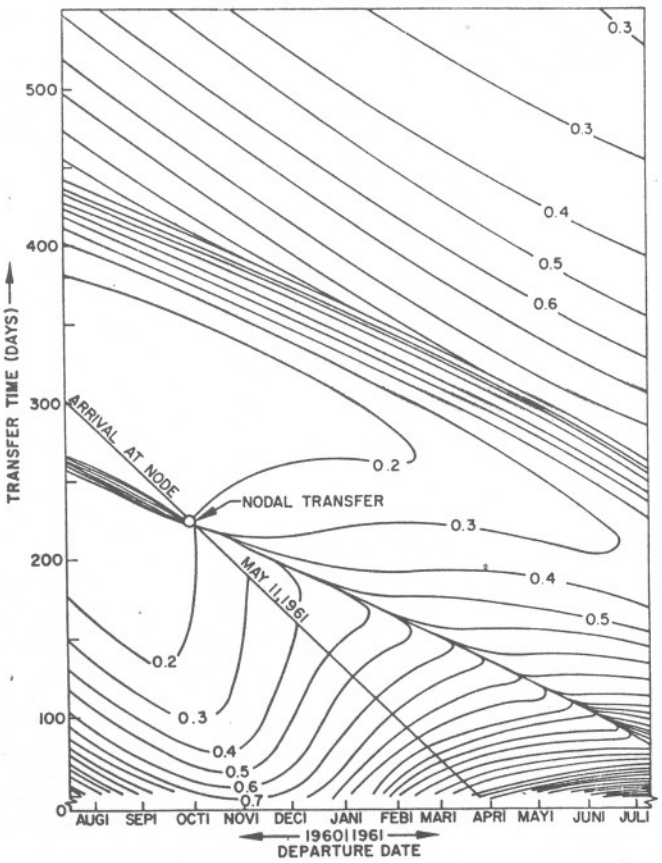

Fig. 6 Mars to Earth. Hyperbolic excess departure speeds (increments of 0.1). Normalized with respect to Earth's mean orbital speed

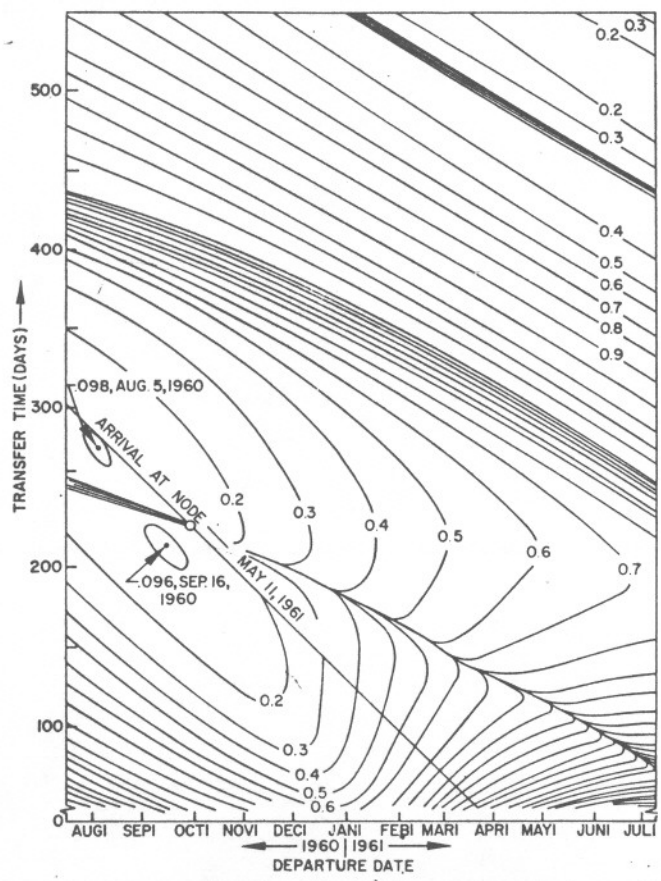

Fig. 7 Mars to Earth. Hyperbolic excess arrival speeds (increments of 0.1). Normalized with respect to Earth's mean orbital speed

This is indeed the case, as inspection of Fig. 6 reveals. Many shorter, physically realistic trips leaving Earth arrive (Fig. 5) at Mars with quite low speeds. When an attempt is made to match a low arrival speed at Mars with an identical departure speed on the same day, it is found that the only return trips for which this is possible are those encompassing longer transit times. Thus, the choice of either a short trip going or a short return trip, but not both, is possible in such cases.

Planning of round trips involves simultaneous manipulation of the various sets of curves, Figs. 3 to 8, until acceptable conditions at all points are realized. These trips will be investigated in a paper now in preparation.

Summary

A useful method of computing interplanetary ballistic transfer orbits and associated planet-centered flight parameters has been presented, along with typical plots of output data. The method is intended for use in:

1 Overall surveys of trajectory requirements, location of trip optima and studies of nonoptimal alternatives to given nominal flights.

2 Indication of local areas of interest for more careful study with precise orbit calculation programs. Using this method as a coarse locator will result in considerable savings of both time and money.

3 Matching of arbitrary planetary escape (or approach) trajectories to the central coasting segment. In this way, the flight planner need not burden himself with the mechanics of an entire flight; instead, his only concern need be how to arrive at (or depart from) "infinity" in a specified direction, possessing a given speed there.

4 Planning of multi-legged journeys and capture orbits in the solar system. Because of the speed and cheapness of the

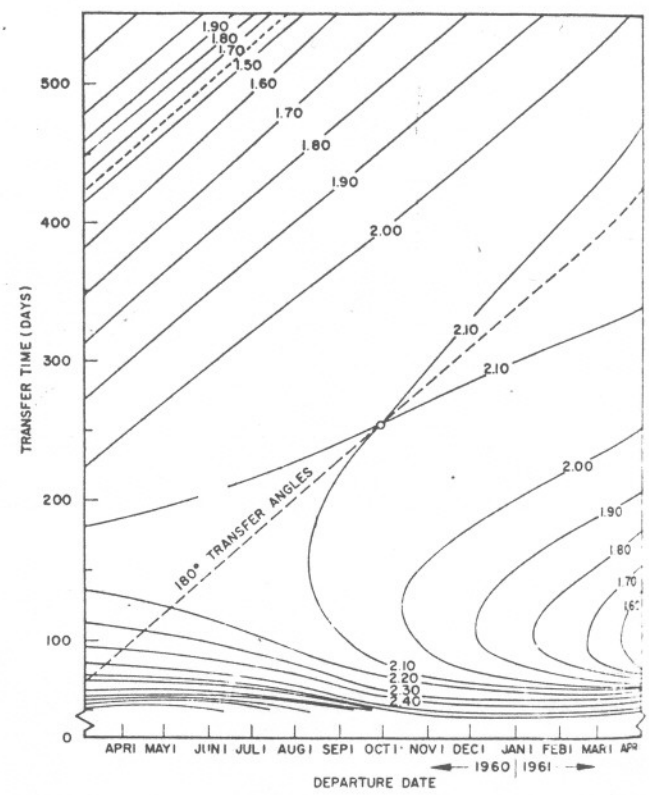

Fig. 8 Earth to Mars, retrograde launchings (co-planar, circular planetary orbits). Hyperbolic excess departure speeds (increments of 0.1). Normalized with respect to Earth's mean orbital speed

calculations, the method represents a most practical way to depict literally thousands of transfers which may be scanned visually or mechanically to find the required components of any broken orbit.

The same method is also applicable to the solution of intercept and rendezvous problems between two satellite orbits about a central body, assuming that oblateness, air drag and other perturbing effects are negligible during the period of transfer.

Acknowledgment

The authors would like to express their sincere appreciation to B. B. Gragg, of Lockheed Missiles and Space Division, for his able assistance in preparing the computer program for the calculations.

Appendix: Kinematical Relations

Heliocentric Orbit

In Fig. 9, geometrical relationships during transfer are illustrated. For any particular trajectory, let S represent the sun, P_1 the planet of departure at the time of departure, P_2 the planet of arrival at the arrival date, and Π_1 and Π_2 the planes of planetary motion. Since the transfer plane Π must contain P_1 and P_2 as well as the sun, and since these three points are, in general, noncollinear, Π is immediately determined. From the diagram, P_1 and P_2 define the angles L_1 and L_2 (both measured eastward from Ω); I, the mutual inclination of the planetary orbits, is a fixed constant. Then, well-known relationships from solid trigonometry yield

$$\cos L = \cos L_1 \cos L_2 + \sin L_1 \sin L_2 \cos I \qquad \text{[A-1]}$$

In order to find all heliocentric orbits which pass through P_1 and P_2 in the stipulated time, it is necessary to investigate not only the two transfer angles L which lie between 0 and 2π, but also all other cases, $L + 2m\pi$, satisfying Equation [A-1].

Now, denote by s the semiperimeter of triangle P_1P_2S (Fig. 10)

$$s = (1/2)(r_1 + r_2 + c)$$

where c, the chord joining P_1 and P_2, is found from

$$c^2 = r_1^2 + r_2^2 - 2r_1r_2 \cos L$$

Let E be given by

$$E = \frac{\text{heliocentric energy of transfer orbit}}{\left|\text{heliocentric energy of elliptic orbit with semimajor axis} = s/2\right|}$$

$$= \begin{cases} -s/2a, \text{ for elliptic transfer} \\ +s/2a, \text{ for hyperbolic transfer} \end{cases}$$

a is the transfer orbit's semimajor (or semitransverse) axis. Finally, let

$$T = \frac{n\Delta t}{(s/2)^{3/2}} = \frac{2\pi \times \text{time of transfer}}{\text{period of elliptic orbit with semimajor axis} = s/2}$$

$\Delta t = t_2 - t_1$; t_1, t_2 are the Julian dates of departure and arrival, and n is the Earth's mean motion.

Then, according to Lambert's theorem (1), the correct elliptic transfer path may be determined by finding E in

$$T = (-E)^{-3/2}[2m\pi + (f - \sin f) - (g - \sin g)] \qquad \text{[A-2]}$$

where

$$\sin^2 f/2 = -E$$
$$\sin^2 g/2 = -EK$$
$$K = 1 - c/s$$

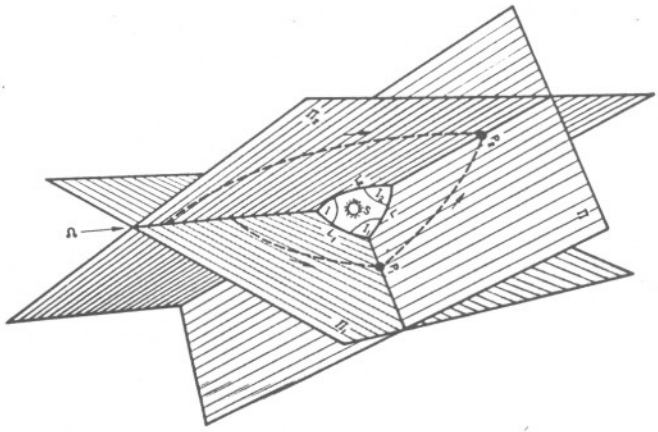

Fig. 9 Transfer geometry

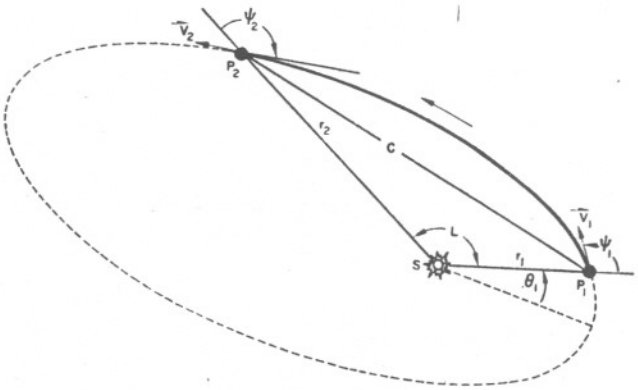

Fig. 10 Relationships in the transfer plane

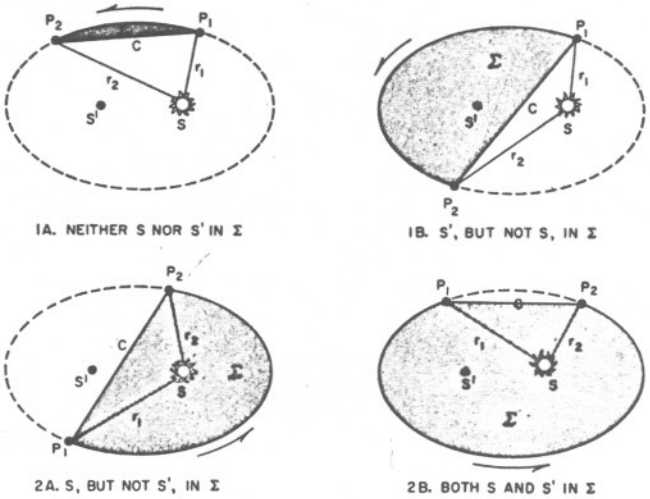

Fig. 11 Different regions for Lambert's theorem

$m = 0, 1, 2, 3, \ldots$ denotes the number of complete circuits on the transfer orbit before P_2 is reached.

These latter equations, however, define f and g ambiguously. It is thus necessary to differentiate among several possible subcases. Σ is the sector bounded by c and the transfer arc; these cases are illustrated in Fig. 11:

Case 1A) $\sin L \geq 0$; neither S nor S' in Σ

$$T = (-E)^{-3/2}[2m\pi + (f - \sin f) - (g - \sin g)] \qquad \text{[A-3]}$$

Case 1B) $\sin L \geq 0$; S', but not S, in Σ

$$T = (-E)^{-3/2}[2(m+1)\pi - (f - \sin f) - (g - \sin g)] \qquad \text{[A-4]}$$

Case 2A) $\sin L \leq 0$; S, but not S', in Σ

$$T = (-E)^{-3/2}[2m\pi + (f - \sin f) + (g - \sin g)] \qquad \text{[A-5]}$$

Case 2B) $\sin L \leq 0$; both S and S' in Σ

$$T = (-E)^{-3/2}[2(m+1)\pi - (f - \sin f) + (g - \sin g)] \qquad \text{[A-6]}$$

where

S' = vacant focus of the transfer orbit
$f = 2 \sin^{-1} \sqrt{(-E)}$
$g = 2 \sin^{-1} \sqrt{(-EK)}$
$E \leq 0$

and $f/2$, $g/2$ are each chosen in $(0, \pi/2)$.

Hyperbolic motion can occur only when $0 \leq L \leq 2\pi$. The appropriate formulas are then:

Case 1H) $0 \leq L \leq \pi$

$$T = (E)^{-3/2}[(\sinh f' - f') - (\sinh g' - g')] \qquad \text{[A-7]}$$

Case 2H) $\pi \leq L \leq 2\pi$

$$T = (E)^{-3/2}[(\sinh f' - f') + (\sinh g' - g')] \qquad \text{[A-8]}$$

where

$E \geq 0$
$f' = 2 \sinh^{-1} \sqrt{E}$
$g' = 2 \sinh^{-1} \sqrt{EK}$

Fig. 12 illustrates curves of E vs. T for representative values of K. The lines drawn for $K = 1$ define regions corresponding to successive values of m. Points lying within the sector marked $m = 2$, for instance, relate to journeys which traverse two complete circuits of the transfer orbit before P_2 is encountered.

As K decreases, each pair of curves, referred to in the foregoing as 1 and 2, draws together, merging finally into the set of dashed lines representing the case $K = 0$. This latter family of orbits is characterized by transfer angles of $L = (2m+1)\pi$.

Where $E = 0$, corresponding elliptic and hyperbolic solutions meet. This situation represents parabolic transfer, and occurs at

$$T_{1a} = (4/3)(1 - K^{3/2}), \text{ for } 0 \leq L \leq \pi$$
$$T_{2a} = (4/3)(1 + K^{3/2}), \text{ for } \pi \leq L \leq 2\pi$$

When S' lies on $\overline{P_1P_2}$, elliptic cases 1A and 1B coincide. This occurs at $E = -1$ (its minimum value), where

$$T_{1b} = (2m+1)\pi - 2 \sin^{-1} \sqrt{K} + 2 \sqrt{K} \sqrt{1 - K}$$
$$\sin L \geq 0$$

Similarly

$$T_{2b} = (2m+1)\pi + 2 \sin^{-1} \sqrt{K} - 2 \sqrt{K} \sqrt{1 - K}$$
$$\sin L \leq 0$$

and E is equal to -1 here also.

Having once specified the constellation of P_1 and P_2, we may immediately form T. And, depending upon its position in relation to T_{1a}, T_{2a}, T_{1b} and T_{2b}, we may then solve for all solutions E which define the various transfer paths. In the region $m = 0$, there exist two, and only two, values of E, for any given T. This is evident from Fig. 12 and can, moreover, be rigorously shown as follows.

To the left of points T_{1b} and T_{2b}, respectively, we find that

$$dT/dE = f(E) \mp K^{5/2} f(EK)$$

according as we consider cases 1H, 1A or 2H, 2A, where

$$f(E) = (3/E^{5/2}) \sinh^{-1} \sqrt{E} - (E+3)/E^2 \sqrt{1+E}$$
$$\text{if } E > 0$$

$$f(E) = [3/(-E)^{5/2}] \sin^{-1} \sqrt{-E} - (E+3)/E^2 \sqrt{1+E}$$
$$\text{if } -1 < E < 0$$

Note that $f(0^+) = f(0^-) = -\frac{2}{5} < 0$, and that $f(E) \to \infty$ as $E \to -1$.

Now, if $E > 0$

$$(d/dE)[E^{5/2} f(E)] = -E^{3/2}/(1+E)^{3/2} < 0$$

Since $0 \leq K < 1$, and $f(0)$ is bounded, it follows that, if $E > 0$

$$E^{5/2} f(E) < (EK)^{5/2} f(EK) \leq 0$$

and, hence, that $dT/dE < 0$, when $E > 1$.

Similarly, when $-1 < E < 0$

$$(d/dE)[(-E)^{5/2} f(E)] = +(-E)^{3/2}/(1+E)^{3/2} > 0$$

so that

$$(-E)^{5/2} f(E) < (-EK)^{5/2} f(EK) \leq 0$$

and, hence, when $-1 < E < 0$

$$dT/dE < 0$$

Since $T \to 0$ as $E \to +\infty$, we observe that as E decreases from $+\infty$ to -1, T increases monotonically from zero to T_{1b}, T_{2b}, respectively. To the right of points T_{1b}, T_{2b}, respectively (in *any* m region, incidentally), on the other hand

$$dT/dE = 3\pi(m+1)(-E)^{5/2} - f(E) \pm K^{5/2} f(EK)$$

which is necessarily positive. Thus, T increases monotonically from T_{1b}, T_{2b}, respectively, to $+\infty$ as E increases from -1 to zero.[6]

The monotonic character of the E,T curves, therefore, establishes the existence of two, and only two, solutions for E, given a particular value of T, in the region $m = 0$. Each successive m region furnishes up to four additional solution

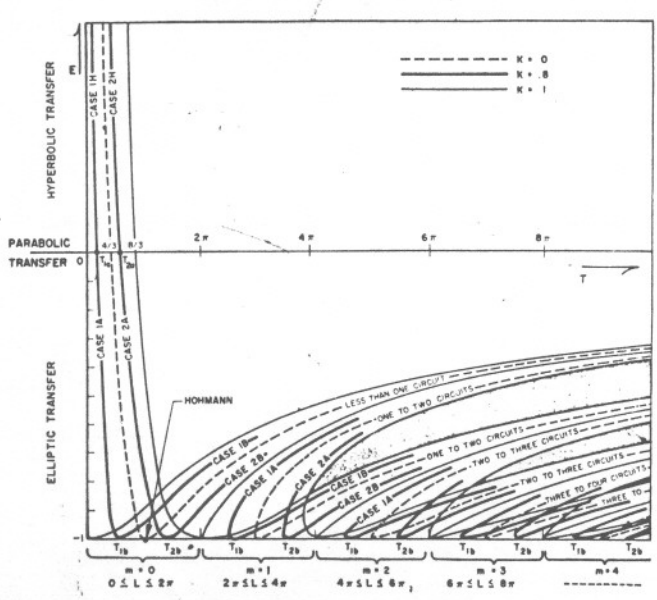

Fig. 12 E vs. T for typical values of K

[6] By somewhat similar arguments, it can be shown that $T'' > 0$ to the left of T_{1b}, T_{2b}, and changes sign just once to the right of these points

corresponding to a given T, depending upon the particular value of K [illegible] ibing the transfer geometry—the higher the [illegible]wer the heliocentric transfer energy.

[illegible]s of E obtained, heliocentric speeds V_1 and V_2, at P_1 and P_2, respectively, may be found from

$$V_1 = \sqrt{2(1/r_1 + E/s)} \qquad V_2 = \sqrt{2(1/r_2 + E/s)}$$

Heliocentric angles of departure and arrival, ψ_1 and ψ_2 (Fig. 10), are determined as follows. For case 1A, for instance (referring to Fig. 13), since the normal at P bisects $\angle SP_1S'$, it follows that

$$(\pi/2) - \psi_1 = (\xi_1 - \eta_1)/2$$

where

$$\xi_1/2 = \tan^{-1}\sqrt{K(s - r_1)/(s - r_2)}$$

$$\eta_1/2 = \tan^{-1}\sqrt{(1 + E)(s - r_2)/(1 + EK)(s - r_1)}$$

principal values of the arc tan being used in each case.

Thus for 1H, 1A

$$\psi_1 = (1/2)(\pi - \xi_1 + \eta_1) \qquad \text{[A-9]}$$

Similarly, for 1B

$$\psi_1 = (1/2)(\pi - \xi_1 - \eta_1) \qquad \text{[A-10]}$$

for 2H, 2A

$$\psi_1 = (1/2)(\pi + \xi_1 + \eta_1) \qquad \text{[A-11]}$$

and for 2B

$$\psi_1 = (1/2)(\pi + \xi_1 - \eta_1) \qquad \text{[A-12]}$$

For each case, the corresponding ψ_2 is obtained by interchanging subscripts 1 and 2 where they occur.

For any given K, the two E,T curves in each m region cross for cases 1B and 2A. From Equations [A-3–A-6] we have

$$E_{(1)} = E_{(2)} = -(\pi/T)^{2/3}$$

independent of m. For these points, from Equations [A-9 through A-12]

$$\psi_{1(1)} = \pi - \psi_{1(2)} \qquad \psi_{2(1)} = \pi - \psi_{2(2)}$$

Both transfer paths (for each value of m), when connected together, form one complete ellipse in space.

Having found E and the velocities at P_1 and P_2, we may now evaluate the remaining heliocentric orbital parameters. They are:

Semimajor axis

$$a = \begin{cases} -s/2E, \text{ elliptic case} \\ +s/2E, \text{ hyperbolic case} \end{cases}$$

Semilatus rectum

$$l = (V_1 r_1 \sin \psi_1)^2 = (V_2 r_2 \sin \psi_2)^2$$

Eccentricity

$$e = \sqrt{1 + 2El/s}$$

Angle of P_1 from perihelion of transfer orbit

$$\theta_1 = \cos^{-1}\{(1/e)(l/r_1 - 1)\} = \sin^{-1}(l \cot \psi_1/r_1 e)$$

Angle of P_2 from perihelion of the transfer orbit is obtained from the foregoing by forming $\theta_2 = \theta_1 + L$.

Calculation of Angular Input Data

Under the assumption that the planetary orbit elements are invariant for the span of time during which flights are con-

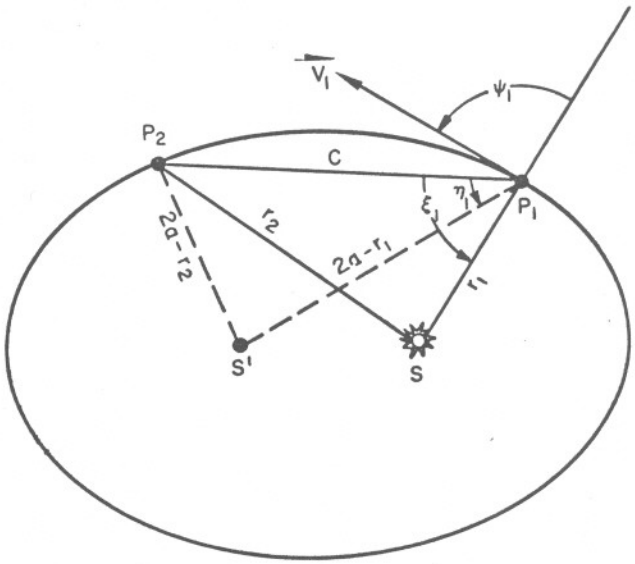

Fig. 13 Determination of ψ_1

templated, there exist relations between departure and arrival dates t_1 and t_2, on the one hand, and the planetary longitudes L_1 and L_2, on the other

$$U_1 = U_{\text{node}} + e_1(\sin U_1 - \sin U_{\text{node}}) + n_1(t_1 - t_{\text{node}}) \qquad \text{[A-13]}$$

where U denotes the eccentric anomaly in the orbit of P_1.

The values of U_{node}, e_1, n_1 and t_{node} are known (7–9), and therefore U_1 is easily calculable. Starting with $U_{1(0)} = U_{\text{node}}$ on the right-hand side, Equation [A-13] is used iteratively. Convergence is quite rapid, since values of e_i in the solar system are small. Then

$$\phi_1 = 2 \tan^{-1}[\sqrt{(1 + e_1)/(1 - e_1)} \tan (1/2)U_1]$$
$$0 \leq \phi_1/2 \leq \pi$$

where ϕ_1 is the true anomaly of P_1. Finally

$$L_1 = \phi_1 - \phi_{\text{node}}$$

ϕ_{node} is also known. Similar formulas are used to obtain L_2 in terms of t_2. Since $\Delta t = t_2 - t_1$, any two of the three quantities t_1, t_2, Δt suffice to determine the third and, hence, the necessary input data.

Conversion to Planetary Coordinates

The foregoing yields values of the heliocentric velocity vectors at the terminal bodies. We now consider each of these vectors to be located essentially at infinity as viewed from its respective planet. Since $\mathbf{V}_1$ is known, we may resolve it into components directed radially from the sun, eastward within and northward from the plane Π_1

$$\mathbf{V}_1 = (V_1 \cos \psi_1,\ V_1 \cos I_1 \sin \psi_1,\ V_1 \sin I_1 \sin \psi_1)$$

where

$$I_1 = \sin^{-1}[\sin I(\sin L_2/\sin L)] =$$
$$\cos^{-1}[(\cos L_2 - \cos L_1 \cos L)/\sin L_1 \sin L]$$

Furthermore

$$\dot{R}_1 = (e_1 \sin \phi_1)/h_1$$

and

$R_1 = r_1 =$ radius vector from S to P_1
$h_1 =$ nondimensional angular momentum of P_1

so that the relative velocity of the departing vehicle, as seen from P_1, is

$$\mathbf{v}_1 = [V_1 \cos \psi_1 - \dot{R}_1,\ V_1 \cos I_1 \sin \psi_1 - (h_1/R_1),\ V_1 \sin I_1 \sin \psi_1] \qquad \text{[A-14]}$$

$$|\mathbf{v}_1| = \sqrt{V_1^2 + \dot{R}_1^2 + (h_1/R_1)^2 - 2V_1(\dot{R}_1 \cos \psi_1 + [h_1/R_1] \cos I_1 \sin \psi_1)}$$

Similar formulas also serve to define $\mathbf{v}_2$.

Equation [A-14] expresses the hyperbolic excess velocity requirement for the launching. That is, $\mathbf{v}_1$ represents the residual velocity vector at "infinity" which the vehicle must possess so that the prescribed heliocentric path be negotiated.

The velocity components are frequently more favorably resolved, however, in terms of a polar-equatorial reference frame than in the heliocentric system of Equation [A-14]. The change of coordinates is effected through two rigid rotations. The first turns $\hat{x}$, the solar radial direction toward P_i, into $\hat{X}$, the direction of the sun's ascending node as viewed in the local planetary equatorial system (for the case of Earth, $\hat{X}$ is directed toward the vernal equinox), through an angle of $\phi_i - \Upsilon_i$.

By the second transformation, ecliptic north $\hat{z}$ is rotated into polar north, $\hat{Z}$, in a left-handed sense about $\hat{X}$, through an equatorial inclination angle i_i, which is a property of the planet in question.

New coordinate axes $\hat{X}$, $\hat{Y}$, $\hat{Z}$ have now been established in the following sense:

- $\hat{X}$ lies in the equatorial plane of P_i, aimed at the sun's ascending node
- $\hat{Z}$ points toward equatorial north
- $\hat{Y}$ completes the right-handed system of coordinates, and the full transformation may be characterized by the single orthogonal matrix

$$D \equiv \begin{pmatrix} \cos(\phi_i - \Upsilon_i) & \sin(\phi_i - \Upsilon_i)\cos i_i & \sin(\phi_i - \Upsilon_i)\sin i_i \\ -\sin(\phi_i - \Upsilon_i) & \cos(\phi_i - \Upsilon_i)\cos i_i & \cos(\phi_i - \Upsilon_i)\sin i_i \\ 0 & -\sin i_i & \cos i_i \end{pmatrix}$$

As seen in the equatorial system of P_i, then, the velocity at infinity is found by matrix multiplication to be

$$\mathbf{v}_i = \mathbf{v}_i \cdot D$$

Finally, the right ascension and declination of $\mathbf{v}_i$ are

$$\alpha_i = \sin^{-1} [(\nu_i)_Y / \sqrt{(\nu_i)_X^2 + (\nu_i)_Y^2}] \qquad 0 \le \alpha_i \le 2\pi$$

$$= \cos^{-1} [(\nu_i)_X / \sqrt{(\nu_i)_X^2 + (\nu_i)_Y^2}]$$

$$\delta_i = \tan^{-1} [(\nu_i)_Z / \sqrt{(\nu_i)_X^2 + (\nu_i)_Y^2}] \qquad -\pi/2 \le \delta_i \le \pi/2$$

References

1 Plummer, H. C., "An Introductory Treatise on Dynamical Astronomy," Cambridge University Press, 1918, *also* Dover Publications, Inc. N. Y., 1960, paperback reprint, chapter V.

2 Battin, R. H., "The Determination of Round-Trip Planetary Reconnaissance Trajectories," *J. Aero/Space Sci.* vol. 26, no. 9, Sept. 1959, pp. 545–567.

3 Gunkel, R. J., Lascody, D. N. and Merrilees, D. S., "Impulsive Midcourse Correction of an Interplanetary Transfer," Proc. Tenth International Astronautical Congress, London, Sept. 1959.

4 Karrenberg, H. K. and Arthur, P. D., "Interplanetary Ballistic Orbits," ARS preprint 870-59, June 1959.

5 Ehricke, K. A., "Zur Auswahl von Flugbahnen für bemannte Raumfahrzeuge zu den Planeten Mars und Venus," *Raketentechnik und Raumfahrtforschung*, Heft 1, Band 4, Jan.–March, 1960, pp. 16–22.

6 Vertregt, M., "Interplanetary Orbits," *J. Brit. Interplanet. Soc.*, vol. 16, no. 6, March–April, 1958, pp. 326–354.

7 "The American Ephemeris and Nautical Almanac for the Year 1960," U.S. Govt. Printing Office, Wash., D. C., 1958.

8 "Planetary Coordinates for the Years 1960–1980," Her Majesty's Stationery Office, London, 1958.

9 "Astronom. Ezheg. SSSR na 1960 g.," *Izdat. Akad. Nauk*, Moscow, 1957, pp. 621–623.

Ballistic Re-Entries With a Varying W/C_DA

R. V. WARDEN[1]

Aeronutronic Div., Ford Motor Co.
Newport Beach, Calif.

An analytical method is presented for evaluating the velocity and deceleration history of a ballistic vehicle experiencing a change in W/C_DA during re-entry. Mass is assumed to be transferred through the process of either ablation or fluid injection into the boundary layer. Vehicle geometry is represented by C_D and A which vary through altitude dependent functions. Gravity and centrifugal forces on the vehicle are neglected, thereby restricting the analysis to large entrance angles and flight velocities. These simplifying assumptions permit a closed form solution of the re-entry trajectory with variable W/C_DA. The governing equation reduces to an incomplete gamma function or exponential integral, depending upon the sign of $d(W/C_DA)/dy$. Results show that the maximum deceleration of the re-entry vehicle is a function of the rate of change of W/C_DA. Furthermore, variable geometry can produce a significant effect on trajectory parameters, such as velocity, deceleration, impact location and heating.

Received May 27, 1960.

[1] Senior Engineer; Project Engineer, Air Force Scout Re-Entry Vehicle. Member ARS.